THE JOURNAL OF BIOLOGICAL CHEMISTRY VOL. 285, NO. 17, pp. 12990–13001, April 23, 2010
© 2010 by The American Society for Biochemistry and Molecular Biology, Inc. Printed in the U.S.A.

Tmem16A Encodes the Ca^{2+}-activated Cl^- Channel in Mouse Submandibular Salivary Gland Acinar Cells*[S]

Received for publication, September 21, 2009, and in revised form, January 30, 2010 Published, JBC Papers in Press, February 22, 2010, DOI 10.1074/jbc.M109.068544

Victor G. Romanenko[‡1], Marcelo A. Catalán[‡1], David A. Brown[‡1,2], Ilva Putzier[§3], H. Criss Hartzell[§], Alan D. Marmorstein[¶‖], Mireya Gonzalez-Begne[**], Jason R. Rock[‡‡4], Brian D. Harfe[‡‡], and James E. Melvin[‡5]

From the [‡]Department of Pharmacology and Physiology and [**]Center for Oral Biology, University of Rochester, Rochester, New York 14642, the [§]Department of Cell Biology, Emory University, Atlanta, Georgia 30322, the [¶]Department of Ophthalmology and Vision Science and [‖]College of Optical Sciences, University of Arizona, Tucson, Arizona 85711, and the [‡‡]Department of Molecular Genetics and Microbiology, University of Florida, Gainesville, Florida 32611

Activation of an apical Ca^{2+}-dependent Cl^- channel (CaCC) is the rate-limiting step for fluid secretion in many exocrine tissues. Here, we compared the properties of native CaCC in mouse submandibular salivary gland acinar cells to the Ca^{2+}-gated Cl^- currents generated by Tmem16A and Best2, members from two distinct families of Ca^{2+}-activated Cl^- channels found in salivary glands. Heterologous expression of Tmem16A and Best2 transcripts in HEK293 cells produced Ca^{2+}-activated Cl^- currents with time and voltage dependence and inhibitor sensitivity that resembled the Ca^{2+}-activated Cl^- current found in native salivary acinar cells. *Best2*$^{-/-}$ and *Tmem16A*$^{-/-}$ mice were used to further characterize the role of these channels in the exocrine salivary gland. The amplitude and the biophysical footprint of the Ca^{2+}-activated Cl^- current in submandibular gland acinar cells from Best2-deficient mice were the same as in wild type cells. Consistent with this observation, the fluid secretion rate in *Best2* null mice was comparable with that in wild type mice. In contrast, submandibular gland acinar cells from *Tmem16A*$^{-/-}$ mice lacked a Ca^{2+}-activated Cl^- current and a Ca^{2+}-mobilizing agonist failed to stimulate Cl^- efflux, requirements for fluid secretion. Furthermore, saliva secretion was abolished by the CaCC inhibitor niflumic acid in wild type and *Best2*$^{-/-}$ mice. Our results demonstrate that both Tmem16A and Best2 generate Ca^{2+}-activated Cl^- current *in vitro* with similar properties to those expressed in native cells, yet only Tmem16A appears to be a critical component of the acinar Ca^{2+}-activated Cl^- channel complex that is essential for saliva production by the submandibular gland.

A Ca^{2+}-activated Cl^- channel (CaCC)[6] is the major apical Cl^- efflux pathway required for fluid secretion in exocrine glands; however, the molecular nature of this channel remains to be determined. Bestrophins (also known as BEST or VMD2) are members of a family of CaCC found in epithelial tissues that express Ca^{2+}-activated Cl^- currents (1–3). The recent discovery of the TMEM16 (also termed ANO) family of CaCC (4–7) introduces additional questions regarding the molecular identity of the epithelial CaCC. Both bestrophin and TMEM16 channels have been shown to generate Ca^{2+}-activated Cl^- currents *in vitro* that are dependent on physiological intracellular Ca^{2+} concentrations (4–6, 8–10).

TMEM16 and BEST Ca^{2+}-activated Cl^- channels (4–6, 8, 11–14) share many of the functional and pharmacological properties of the CaCC expressed in native secretory cells (15–18), unlike the other putative Ca^{2+}-activated Cl^- channels, *i.e.* CLCA, CLC3, and TWEETY (19–22). Silencing of TMEM16A by small interfering RNA transfection inhibited the short circuit current due to Ca^{2+}-dependent Cl^- secretion in primary cultures of human bronchial epithelial cells and in the pancreatic cell line CFPAC-1 (4), as well as the swell-activated, Ca^{2+}-dependent current in numerous cell lines (23). However, expressed mouse Tmem16A was markedly more sensitive to a panel of anion channel blockers than the CaCC found in native secretory cells, and importantly, knockdown of Tmem16A produced only a modest effect (~25% inhibition) on saliva secretion (6) raising the possibility that another CaCC is present in salivary gland acinar cells. Similarly, small interfering RNA to Best1 suppressed endogenous Ca^{2+}-activated Cl^- currents in airway and colonic epithelial cells (1, 24), whereas expression of Best1 transcripts and CaCC activity were up-regulated in neurons following injury (7), implying that *Best1* encodes a Ca^{2+}-activated Cl^- channel in these various cell types. Nevertheless, the Ca^{2+}-activated Cl^- current in the retinal pigment epithelium of *Best1* null mice is normal (25). Accordingly, the functioning of bestrophins in native tissue as Ca^{2+}-dependent Cl^- channels remains controversial (11, 22). These results suggest that the Ca^{2+}-activated Cl^- current in salivary gland acinar

* This work was supported, in whole or in part, by National Institutes of Health Grants DE09692 and DE08921 (to J. E. M.), GM060448 (to H. C. H.), and EY13160 (to A. D. M.). This work was also supported by the Macular Vision Research Foundation (to A. D. M.) and an unrestricted grant to the Department of Ophthalmology and Vision Science at the University of Arizona from Research to Prevent Blindness (to A. D. M.).

[S] The on-line version of this article (available at http://www.jbc.org) contains supplemental Fig. 1.

[1] These authors contributed equally to this work.

[2] Supported by National Institutes of Health Training Grant DE07202 from NIDCR (to J. E. M.).

[3] Present address: Dept. of Pharmacology and Chemical Biology, University of Pittsburgh, Pittsburgh, PA 15261.

[4] Present address: Dept. of Cell Biology, Duke University Medical Center, Durham, NC 27710.

[5] To whom correspondence should be addressed: Dept. of Pharmacology and Physiology, University of Rochester Medical Center, Box 711, 601 Elmwood Ave., Rochester, NY 14642. Tel.: 585-275-3444; Fax: 585-273-2652; E-mail: james_melvin@urmc.rochester.edu.

[6] The abbreviations used are: CaCC, Ca^{2+}-activated Cl^- channel; CAPS, 3-(cyclohexylamino)propanesulfonic acid; SMG, submandibular gland; DIDS, 4,4′-diisothiocyanatostilbene-2,2′-disulfonate; NFA, 2-[3-(trifluoromethyl)anilino] nicotinic acid (niflumic acid); A9C, anthracene-9-carboxylic acid; PIPES, 1,4-piperazinediethanesulfonic acid; CCh, carbachol; X-gal, 5-bromo-4-chloro-3-indolyl-β-D-galactopyranoside.

cells may involve multiple channels, possibly including a TMEM16 and/or a BEST family member. Consequently, it is important to determine whether other Ca^{2+}-activated Cl^- channels, including members of the *TMEM16* and *BEST* families, are important in the functional formation of the Ca^{2+}-activated Cl^- channel complex in the exocrine salivary gland and other organ systems.

The human bestrophin gene family consists of four members, *BEST1–4* (also known as *VMD2* and *VMD2L1–L3,* respectively) (10, 26, 27), whereas the Tmem16 family has 10 members, TMEM16A–TMEM16K (or ANO1–ANO10) (6, 28). Three functional bestrophin homologues are present in the mouse genome (29). *Best3* generates numerous splice variants in tissues such as the mouse brain, retina, kidney (29), and salivary glands (9). Salivary gland acinar cells express Best2, but not Best1, as well as Best3-Δ2,3,6, a splice variant of the Best3 Ca^{2+}-dependent Cl^- channel (9). Because it lacks 132 amino acids in the critical N-terminal domain (30, 31), Best3-Δ2,3,6 does not produce Ca^{2+}-dependent Cl^- currents, nor does it regulate Best2 channel activity (9). If a bestrophin codes for the CaCC current in the exocrine salivary gland, it is not likely to be *Best3*. Therefore, we have focused on *Best2* in this study. On the other hand, TMEM16A protein is also detected in exosomes isolated from human parotid saliva (32) as well as in the apical membrane of mouse salivary gland acinar cells (6), suggesting that this channel may be part of the Ca^{2+}-activated Cl^- channel complex in salivary gland cells.

To explore these possibilities, we evaluated the role of the Tmem16A and Best2 channels in the exocrine mouse submandibular salivary gland. Heterologous expression of mouse Tmem16A and Best2 generated Ca^{2+}-activated Cl^- currents with similar properties to those expressed in native mouse salivary gland acinar cells. Nevertheless, disruption of *Best2* failed to change the properties of the Ca^{2+}-activated Cl^- current in acinar cells or the fluid secretion rate in these mice. In contrast, *Tmem16A*$^{-/-}$ mice lacked stimulated Cl^- efflux, an index of fluid secretion, and Ca^{2+}-activated Cl^- current. We conclude that Tmem16A, but not Best2, is an important functional element of the Ca^{2+}-activated Cl^- channel complex in submandibular gland acinar cells.

EXPERIMENTAL PROCEDURES

General Methods—*Tmem16A*$^{-/-}$ and *Best2*$^{-/-}$ mice were generated and maintained as described previously (33, 34). Mice were housed in micro-isolator cages with *ad libitum* access to laboratory chow and water during 12-h light/dark cycles. Gender- and age-matched (2–6 months old) littermate wild type and *Best2*$^{-/-}$ animals were utilized. Because few *Tmem16A*$^{-/-}$ mice survive more than 4 days past birth, 2–3-day-old mice were used (34). C57BL/6 strain mice were obtained from The Jackson Laboratories (Bar Harbor, ME), the strain on which the *Best2*$^{-/-}$ and *Tmem16A*$^{-/-}$ mice were maintained. All experimental protocols were approved by the University of Rochester Animal Resources Committee. Mice were rendered unconscious by exposure to CO_2 and then killed by exsanguination prior to removal of the submandibular glands. Reagents were obtained from Sigma unless otherwise specified.

Heterologous Expression of Mouse Tmem16A and Best2—To characterize their function, mouse Tmem16A and Best2 were expressed in HEK293 cells (HEK293-Tmem16A and HEK293-Best2, respectively), a cell line that endogenously expresses little if any *Tmem16A* or *Best2*. HEK293 cells were maintained in growth medium (Dulbecco's modified Eagle's medium supplemented with 10% fetal bovine serum) containing nonessential amino acids (0.1 mM), sodium pyruvate (1 mM), L-glutamine (2 mM), penicillin and streptomycin (100 μg/ml of each antibiotic) at 37 °C in a 5% CO_2 atmosphere humidified incubator. Reagents were obtained from Invitrogen.

Best2-inducible HEK293 cells were engineered with the insertion of a single copy of the Best2 cDNA into the genome (supplemental Fig. 1*A*). Best2 expression was induced by addition of tetracycline (2 μg/ml) to the growth medium. After induction, the cells expressed Best2 mRNA as detected by reverse transcriptase-PCR (supplemental Fig. 1*B*). Patch clamp analysis revealed currents that were stimulated by intracellular Ca^{2+} and reversed near E_{Cl} as expected for a Cl^- current. No CaCC current was detected in non-tetracycline-induced HEK293-Best2 cells (Fig. 2*B*, see *arrow*).

Primers (Integrated DNA Technologies, Coralville, IA) containing KpnI and BamHI restriction sites (underlines) were used to amplify the Tmem16A transcript from mouse (C57BL/6) submandibular gland cDNA for insertion into pcDNA3.1$^+$ (Invitrogen). PCRs were performed using Platinum®-*Pfx* DNA polymerase (Invitrogen) following the manufacturer's protocol. The PCR products were digested and ligated into pcDNA3.1$^+$ at the KpnI and BamHI sites and verified by direct sequencing. The primers were from 5′ to 3′, forward, GAGGCCGGTACCATGAGGGTCCCCGAGAAGTACTCGACG, and reverse, ACCGGATCCCTACAGCGCGTCCCCATGGTACTC.

HEK293-based Flp-In™ 293 cells (Invitrogen) were transiently co-transfected with the mouse Tmem16A-pcDNA3.1$^+$ construct (0.1 μg) and pmaxGFP (for positive visualization of transfected cells; 0.25 μg; Lonza, Walkersville, MD), using Lipofectamine 2000 (Invitrogen) as described previously (35). Transfected cells were incubated in 5% CO_2 at 37 °C overnight, and experiments were performed the next day.

β-Galactosidase Staining—The *Best2* gene was disrupted by targeted insertion of the *lacZ* gene, replacing exons 1, 2, and part of exon 3 (33). Consequently, expression of LacZ is driven by the *Best2* promoter, permitting detection of the endogenous Best2 expression pattern. The submandibular glands were fixed in 0.2% paraformaldehyde in 0.1 M PIPES, pH 6.9, at 4 °C. Tissues were rinsed in phosphate-buffered saline, equilibrated in 30% sucrose overnight, and embedded in Tissue-Tek (Sakura Finetek) for sectioning. Frozen sections of 7 μm were post-fixed in 0.2% paraformaldehyde on ice for 10 min, rinsed in phosphate-buffered saline with 2 mM $MgCl_2$, and processed for β-galactosidase staining as described previously (36).

Immunolocalization—Immunostaining was performed essentially as described previously (37). Briefly, endogenous biotin was blocked using an Avidin/Biotin blocking kit (Vector Laboratories, Burlingame, CA). After biotin blocking, sections stained for LacZ as above were incubated overnight with a rabbit anti-peptide polyclonal antibody (1:500 dilution) directed to

a 17-amino acid sequence in the cytoplasmic region of rat AQP5 (Calbiochem). For Tmem16A immunolocalization, submandibular glands from 2- to 3-day-old and 2- to 3-month-old adult mice were fixed with Bouin's fixative and paraffin-embedded (37). Sections were incubated overnight with a rabbit anti-peptide polyclonal antibody (1:1000 dilution) directed to an amino acid sequence (residues 451–466; KDHPRAEYEARVLEKS) flanked by putative transmembrane domains 2 and 3 in the mouse Tmem16A protein (AbFrontier Co., Seoul, Korea). Bound immunoglobulin was detected with the Vectastain Elite ABC kit (Vector Laboratories), and peroxidase was visualized by incubation with 3,3′-diaminobenzidine (Vector Laboratories).

Ex Vivo Submandibular Gland (SMG) Perfusion—*Ex vivo* SMG perfusion was performed essentially as reported previously (38). The perfusion solution contained (in mM) the following: 4.3 KCl, 120 NaCl, 25 $NaHCO_3$, 5 glucose, 10 HEPES, 1 $CaCl_2$, 1 $MgCl_2$, pH 7.4. Solutions maintained at 37 °C were gassed with 95% O_2, 5% CO_2 and perfused at 0.8 ml/min using a peristaltic pump. The *ex vivo* gland was stimulated with a combination of muscarinic and β-adrenergic receptor agonists (0.3 μM carbachol and 5 μM isoproterenol, respectively). Once the gland began to secrete fluid (defined as time 0), stimulation was continued for an additional 10 min. Saliva was collected in precalibrated capillary tubes (Sigma), and volumes were recorded every minute to calculate the flow rate (μl/min). The pH was measured at the end of the saliva collection period using a pH electrode (Thermo Scientific, Beverly, MA). *Ex vivo* saliva samples were then stored at −86 °C until further analysis. Na^+ and K^+ concentrations were analyzed by atomic absorption using a 3030 spectrophotometer (PerkinElmer Life Sciences). The Cl^- concentration was analyzed with an Expandable Ion Analyzer EA 940 (Orion Research).

Plasma Membrane Protein Isolation and Western Blot Analysis—A 75-cm^2 flask of Flp-In™-293 cells was transiently transfected with either Tmem16A-pcDNA3.1$^+$ or pcDNA3.1$^+$ (empty vector). Cells were incubated 48 h post-transfection with 0.25 mg/ml EZ-Link® Sulfo-NHS-SS-Biotin (Pierce) in ice-cold phosphate-buffered saline for 30 min at 4 °C as described previously (35). Scraped cells were centrifuged at 500 × *g* for 3 min (Allegra® X-15R Centrifuge, Beckman Coulter; Fullerton, CA), and the resultant pellet was lysed on ice for 30 min in 150 μl of lysis buffer containing Halt protease inhibitor mixture (Pierce), followed by sonication (Sonifier S-450A; Branson, Danbury, CT) and centrifugation at 10,000 × *g* for 2 min at 4 °C. The supernatant was incubated with NeutrAvidin beads (Pierce) for 60 min at 4 °C. Bound biotinylated proteins were released by adding SDS-PAGE sample buffer containing 50 mM dithiothreitol.

Crude plasma membranes from submandibular salivary glands from C57BL/6 and *Best2*$^{-/-}$ mice were isolated as before (37). Minced glands were suspended in 1 ml of ice-cold homogenizing buffer containing 250 mM sucrose (J. T. Baker Inc.), 10 mM triethanolamine, 1 μg/ml leupeptin, and 0.1 mg/ml phenylmethylsulfonyl fluoride. Cells were homogenized with a glass-Teflon tissue grinder and centrifuged at 4,000 × *g* for 10 min at 4 °C. The supernatant was saved, and the pellet was resuspended and centrifuged in the same volume of homogenization buffer as before. The collected supernatants were pooled and centrifuged at 22,000 × *g* for 20 min at 4 °C. The pellet was suspended in the same buffer and centrifuged at 46,000 × *g* (Beckman Coulter SW28 Ti rotor) for 30 min at 4 °C to obtain the crude plasma membrane fraction.

For Western blot analysis, 50 μg of the submandibular crude plasma membrane fraction or 15 μg of the biotinylated fraction from transfected Flp-In™-293 cells were heated at 55 °C for 20 min prior to separation in a 10% SDS-PAGE Tris-glycine minigels (Bio-Rad). Protein was transferred overnight at 4 °C onto polyvinylidene difluoride membranes (Invitrogen) using a transfer buffer containing 10 mM CAPS, pH 11, in 10% methanol. Membranes were blocked overnight at 4 °C with 5% nonfat dry milk in 25 mM Tris, pH 7.5, 150 mM NaCl (TBS) prior to incubation with anti-Tmem16A antibody (Open Biosystems, Huntsville, AL) at 1:500 dilution, in TBS, 2.5% nonfat dry milk solution at 4 °C overnight. The rabbit anti-peptide polyclonal antibody was generated by simultaneous introduction of three unique amino acid sequences of mouse Tmem16A located between the predicted transmembrane domains TM2 and TM3 (FEEEEDHPRAEYEARVLEKSLR) and between domains TM5 and TM6 (MEECAPGGCLMELCIQL and DREEYVKRKQRYEVDFNLE). After washing with Tris-buffered saline containing 0.05% Tween 20 (TBS-T), the membranes were incubated with horseradish peroxidase-conjugated goat anti-rabbit IgG secondary antibody (Pierce) at a dilution of 1:2500 in TBS-T, 2.5% nonfat dry milk for 1 h at room temperature. Labeled proteins were visualized by enhanced chemiluminescence (ECL detection kit; GE Healthcare).

Electrophysiological Recordings—Single cells were prepared from mouse submandibular glands as described previously for acinar (39) and for granular duct (38) cells. Voltage clamp experiments were performed using the standard whole-cell patch clamp technique at room temperature. Electrophysiological data were acquired using a PC-501A amplifier (Warner Instrument, Hamden, CT) or an Axopatch 200B amplifier (Molecular Devices, Sunnyvale, CA). Voltage pulses were generated with Clampex 9 software through a Digidata 1320A interface (Molecular Devices, Sunnyvale, CA), which also served to acquire the currents. Pipettes from Corning 8161 patch glass (Warner Instrument, Hamden, CT) were pulled to give a resistance of 3–5 megohms in the solutions described below. Ca^{2+}-activated Cl^- currents were recorded in an external solution containing (in mM) the following: 155 tetraethylammonium Cl, 2 $CaCl_2$, 1 $MgCl_2$, 10 HEPES, pH 7.2, and the pipette solution contained the following: 60 tetraethylammonium Cl, 90 tetraethylammonium glutamate, 5 Ca^{2+}-EGTA, 10 HEPES, pH 7.2. The level of free Ca^{2+} was varied between 0 and 2.5 μM, estimated using the WEBMAXC calculator website. In some experiments, the extracellular Cl^- (150 mM) was substituted with Br^-, I^-, NO_3^-, or glutamate. In other experiments, the external solution was supplemented with a Cl^- channel inhibitor, 2-[3-(trifluoromethyl)anilino] nicotinic acid (NFA, niflumic acid), 4,4′-diisothiocyanatostilbene-2,2′-disulfonate (DIDS), or anthracene-9-carboxylic acid (A9C) at various concentrations or with 1 μM of the Ca^{2+} ionophore ionomycin. In a significant fraction of HEK293 cells, a transient anion current was observed in addition to the CaCC

current. This current, which usually disappeared within 15 min after breakthrough, showed biophysical (*i.e.* weak outward rectification and slow inactivation at positive potentials) and pharmacological properties like VRAC, the volume-activated anion current (40, 41). Recording of CaCC current was performed only in the absence of VRAC as evidenced by the lack of both voltage-dependent inactivation at positive potentials and sensitivity of the current to 100 μM suramin (40).

The relative anion permeability was determined using the GHK equation (42) modified as follows: $P_X/P_{Cl} = [Cl^-]_o^b/([X]_o \exp(\Delta E_{rev}F/RT)) - [Cl^-]_o^a/[X]_o$, where $[Cl^-]_o^b$ and $[Cl^-]_o^a$ are the chloride concentrations before and after extracellular anion replacement; ΔE_{rev} is the resultant reversal potential shift, and F, R, and T have their conventional thermodynamic meanings. The measured reversal potentials were corrected for the computed liquid junction potentials (Clampex, Molecular Devices, Sunnyvale, CA). The effectiveness of channel inhibitors was evaluated by constructing the dose-response curve using the following equation: $I = (I_{max} - I_{min})/((IC_{50}/[Inh])^n + 1)$, where I_{max} and I_{min} are the maximum or minimum current amplitudes, [Inh] is the inhibitor concentration, IC_{50} is the [Inh] to block 50% of the current, and n is the Hill coefficient. The $[Ca^{2+}]$ dependence of the currents was fitted with the Hill equation of the form $I = I_{max}/\{1 + 10\wedge((\log EC_{50} - \log[Ca^{2+}])^n)\}$, where EC_{50} is the concentration of Ca^{2+} that produces half-maximal activation of the channels, and n is the Hill coefficient, and F-test was used for comparison. Statistical analyses were done using Prism (GraphPad, La Jolla CA). Note that the distribution of the best fit EC_{50} is not Gaussian, whereas the distribution of $\log EC_{50}$ passes the normality test (43). Therefore, the data were fit to the Hill equation written in terms of $\log EC_{50}$ rather than EC_{50}, and the standard errors are provided for $\log EC_{50}$ values but not for EC_{50} values. Fitting and statistical analyses were performed using either Clampfit (Molecular Devices, Sunnyvale, CA), Origin (Origin Labs, Northampton, MA), or Prism (GraphPad, La Jolla CA) software.

$[Ca^{2+}]_i$ and $[Cl^-]_i$ Measurements—SMG acinar cells were isolated from age-matched littermate mice (*Tmem16A*$^{+/+}$, *Tmem16A*$^{+/-}$, and *Tmem16A* $^{-/-}$) 2–3 days post-birth and prepared as described above (see under "Electrophysiological Recordings"). The fluorescent dyes Fura-2 and SPQ were used essentially as described previously for $[Ca^{2+}]_i$ (44) and $[Cl^-]_i$ (45, 46) measurements, respectively. Cells were loaded with dye by incubation with either 2 μM Fura-2 AM (Invitrogen) for 10–20 min at room temperature or 5 mM SPQ (Molecular Probes) for 30 min at 37 °C. Imaging was performed using an inverted microscope (Nikon Diaphot 200) equipped with an imaging system (Till Photonics, Pleasanton, CA). Images were acquired at a rate of 1 Hz by alternate excitation at 340 and 380 nm (Fura-2) or excitation at 344 nm (SPQ), and emission captured at 510 nm using a high speed digital camera (Till Photonics). Chamber volume was maintained at ~400 μl. Cells were superfused at a rate of 4 ml/min with the *ex vivo* perfusion solution at 37 °C. For $[Ca^{2+}]_i$ measurements, the fluorescence ratio of 340 nm over 380 nm was calculated, and all data were presented as the change in ratio units. $[Cl^-]_i$ data are presented as F_0/F units essentially as described previously (45, 46), a ratio generated by dividing the average fluorescence during the 1-min time period obtained at rest just prior to stimulation (F_0) by the fluorescence values (F) obtained throughout the experiment.

Statistical Analyses—Results are presented as the mean ± S.E. Statistical significance was determined using unpaired Student's t tests where appropriate. Two-tailed p values of less than 0.05 were considered statistically significant. With more than two groups, statistical analysis was made by one-way analysis of variance. The post hoc Bonferroni test was applied with a threshold for statistical significance of $p < 0.05$. All experiments were performed using three or more separate preparations.

RESULTS

Ca^{2+}-activated Cl^- Currents in Submandibular Acinar Cells and HEK293 Cells Expressing Mouse Tmem16A and Best2—A CaCC is the major apical Cl^- efflux pathway activated during fluid secretion in exocrine salivary glands; however, the molecular nature of this channel is unknown (47). Previous reports demonstrate that members of the *TMEM16* (4–7) and *BEST* (8, 11–13) gene families encode Ca^{2+}-activated Cl^- channels with properties much like those found in native tissues (1, 15–18). TMEM16A was previously detected in a proteomics screen of exosomal proteins isolated from human parotid saliva (32) and in the apical membrane of mouse salivary acinar cells (6), whereas mouse salivary gland acinar cells express transcripts for Best2 (9). These studies suggest that one or both of these channels might contribute to the Ca^{2+}-activated Cl^- channel complex in salivary gland acinar cells. Direct sequencing confirmed that the Tmem16A and Best2 transcripts from the mouse submandibular salivary gland are identical to those reported previously (Tmem16A(a,c) splice variant, NCBI accession number Q8BHY3; Best2, NCBI accession number BC031186).

We next compared the properties of the CaCC currents generated in HEK293 cells expressing either mouse Tmem16A (HEK293-Tmem16A) or Best2 (HEK293-Best2) to those in native mouse SMG acinar cells. It is often difficult to directly compare the results from studies of CaCC currents in native cells and expression systems because of the many different conditions and protocols employed (*e.g.* compare the different properties of expressed Best2 in Fig. 1*C* with those in Ref. 9). To control for such differences, we have used identical experimental conditions. Fig. 1 illustrates the general similarity of the CaCC currents in mouse SMG acinar cells (Fig. 1*A*) and in HEK293 cells expressing Tmem16A (Fig. 1*B*) or Best2 (Fig. 1*C*). The CaCC current activated by 250 nM internal Ca^{2+} was recorded from a holding potential of −50 mV during voltage clamp steps from −80 to +120 in 20-mV increments. All three cells displayed hallmarks of epithelial CaCC currents, including slow time-dependent current activation, de-activating tail currents upon repolarization (*upper panels*, Fig. 1, *A–C*), and strong outward rectification (current plotted is Cl^- current at the end of the pulse; *filled symbols*, *lower panels*, Fig. 1, *A–C*). Note that the CaCC currents were effectively inhibited by the Ca^{2+}-activated Cl^- channel blocker NFA (100 μM; *open sym-*

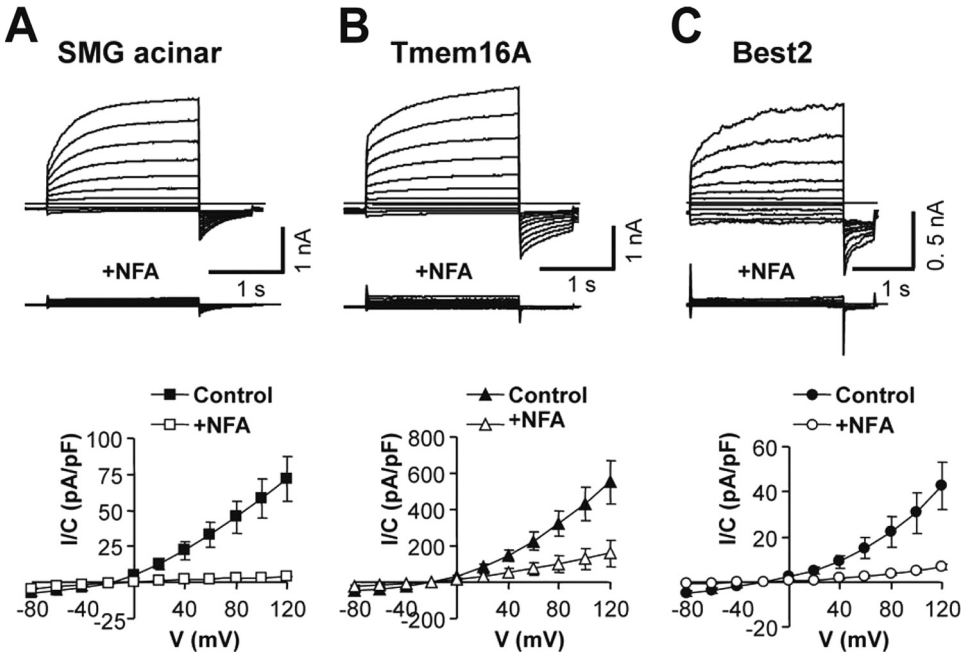

FIGURE 1. **Comparison of native SMG acinar, Tmem16A, and Best2 CaCC currents.** CaCC currents were activated with an internal Ca^{2+} concentration of 250 nM and recordings made of currents 1–5 min after achieving the whole-cell configuration in adult mouse submandibular acinar cells (*SMG acinar*, *A*) and in HEK293 cells expressing either Tmem16A (*Tmem16A*, *B*) or Best2 (*Best2*, *C*). Current was recorded during 2-s voltage steps (20 mV) from −80 to +120 (from a holding potential of −50 mV) followed by a 0.5-s step to −80 mV. Representative time courses of the currents are shown in the *upper panels*. The current-voltage relations determined at the end of each test pulse are shown in the *lower panels* ($n = 4–6$ cells for each condition). The *middle* and *lower panels* also show that the CaCC currents in SMG acinar, HEK293-Tmem16A, and HEK293-Best2 cells were strongly inhibited by superfusion of the Ca^{2+}-activated Cl^- channel blocker NFA (100 μM).

bols) in SMG acinar, HEK293-Tmem16A, and HEK293-Best2 cells (Fig. 1, *A–C*, respectively).

Collectively, the close resemblance of the Ca^{2+}-activated Cl^- currents presented in Fig. 1, *A–C,* suggested that the endogenous CaCC current in mouse SMG acinar cells may be generated by Tmem16A and/or Best2. Further investigations of the functional properties of expressed Tmem16A and Best2 were consistent with this premise (Fig. 2). The normalized current-voltage relations of the CaCC current activated by 250 nM internal Ca^{2+} for the three cell types showed strong outward rectification that overlapped, indicating that their voltage dependence was comparable (Fig. 2*A*). Note also that the normalized current-voltage relation of the CaCC current activated by high internal Ca^{2+} (1 μM) was nearly linear in SMG acinar, HEK293-Tmem16A, and HEK293-Best2 cells (Fig. 2*A*, *inset*), another characteristic property of epithelial CaCC currents. The Ca^{2+} sensitivities of the CaCC currents generated by expressed Tmem16A and Best2 were in the physiological range and quite similar to that observed in native SMG acinar cells (Fig. 2*B*, *filled symbols*). High internal Ca^{2+} (1000 nM) failed to activate a CaCC current in HEK293-Best2 cells that had not been induced to express Best2 with tetracycline or in HEK293 cells transfected with green fluorescent protein (Fig. 2*B*, *open symbols, arrow*). The anion permeability sequence of SMG acinar cells was the same as expressed Tmem16A and Best2 (Fig. 2*C*, $I^- > NO_3^- > Br^- > Cl^- \gg$ glutamate), but SMG acinar cells were more selective (*i.e.* the P_X/P_{Cl} was significantly greater for I^-, NO_3^-, and Br^- in SMG cells). All three cell types were sensitive to the anion channel blockers NFA, A9C, and DIDS (Fig. 2*D*). However, the IC_{50} value for Tmem16A was significantly greater in each case (note log scale) compared with native CaCC. The IC_{50} value for the CaCC current in HEK293-Tmem16A cells was quite different from the sensitivity to these blockers reported in an earlier study for expressed Tmem16A (6).

Characterization of Submandibular Gland Function in Best2-deficient Mice—Based on the general similarities between the CaCC currents in native salivary gland acinar, HEK293-Best2, and HEK293-Tmem16A cells, we predicted that the Best2 and/or Tmem16A channel might be critical to the fluid secretion process. We took advantage of *Best2* null mice (33) lacking functional regions critical for Best Ca^{2+}-activated Cl^- channel activity (12, 48) and an *ex vivo* mouse submandibular protocol (38) to directly test the role of the Best2 Cl^- channel in salivary gland fluid secretion. $Best2^{-/-}$ mice grew normally and were fertile (33), and there was no change in the adult weight of the submandibular gland ($Best2^{-/-}$, 58.3 ± 7.9 mg; $Best2^{+/+}$, 54.5 ± 7.2 mg; $n = 9$ for each group; $p > 0.7$). PCR primers failed to amplify the 5′-deleted region in $Best2^{-/-}$ mice, confirming that intact Best2 transcript is not generated (33). Despite the loss of Best2 expression, submandibular glands from mice lacking Best2 secreted saliva with nearly identical kinetics (Fig. 3*A*, *open symbols*) and with a comparable total amount of saliva as wild type controls ($Best2^{-/-}$, 121 ± 8 μl/10 min; $Best2^{+/+}$, 124 ± 11 μl/10 min; $n = 8$ for each group; $p > 0.8$). Therefore, Best2 appeared not to be involved in transepithelial salivary gland Cl^- movement, the driving force for fluid secretion (47, 49). One possible explanation for the apparent lack of effect of *Best2* disruption on salivary gland secretion is that compensation may have occurred, particularly enhanced expression of Tmem16A. However, expression of Tmem16A protein was comparable in the plasma membrane of $Best2^{-/-}$ and wild type mice (Fig. 3*B*, *left panel*). Note that the apparent size of Tmem16A expressed in HEK293 cells was similar to the native protein and that no signal was observed in HEK293 cells transfected with an empty vector (Fig. 3*B*, *right panel*), confirming the specificity of the antibody and the lack of native Tmem16A in HEK293 cells.

The results shown in Fig. 3 suggested that it is unlikely that the Best2 Ca^{2+}-activated Cl^- channel contributes much to the generation of a Cl^- current in native salivary gland acinar cells. To directly test this possibility, we examined the CaCC current in submandibular acinar cells isolated from $Best2^{-/-}$ mice. Such studies revealed that the fundamental characteristics

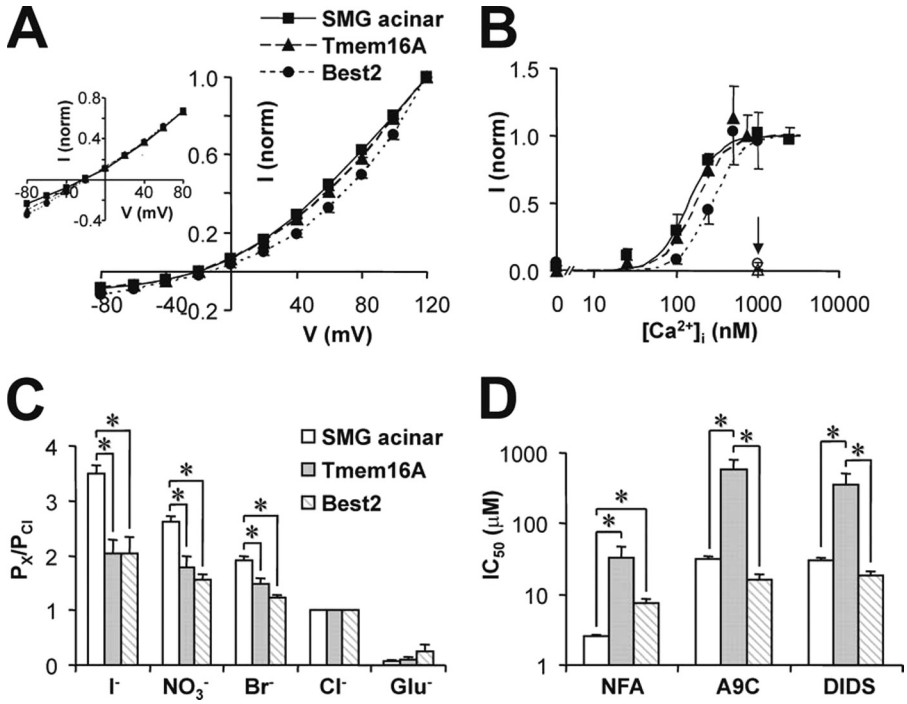

FIGURE 2. **Biophysical properties of the CaCC currents in SMG acinar, Tmem16A-expressing, and Best2-expressing HEK293 cells.** CaCC currents were recorded from adult mouse submandibular acinar cells (*SMG acinar*) and HEK293 cells expressing either Tmem16A (*Tmem16A*) or Best2 (*Best2*) cells using the same voltage protocol as in Fig. 1. *A,* comparison of the current-voltage relations were made on CaCC currents activated by 250 nM internal $[Ca^{2+}]$. The currents determined at the end of the pulses were normalized by the current elicited at +120 mV. Data were obtained from $n = 8–9$ cells. *Inset*, normalized CaCC current activated by 1000 nM internal $[Ca^{2+}]$ (note that the current-voltage relations become nearly linear in all three cell types). *B,* dependence of the CaCC current on internal $[Ca^{2+}]$ was evaluated using concentrations ranging from near 0 to 2500 nM (*filled symbols*). The absence of CaCC current (*arrow*) is demonstrated in green fluorescent protein-transfected HEK293 cells (*open triangle*) and HEK293-Best2 cells unexposed to tetracycline (*open circle*) patched with 1000 nM $[Ca^{2+}]$ in the pipette solution ($n = 3–34$ cells). Lines were fit to the Hill equation to determine the EC_{50}: SMG $EC_{50} = 126$ nM ($logEC_{50} = 2.10 \pm 0.08$); Tmem16A $EC_{50} = 196$ nM ($logEC_{50} = 2.29 \pm 0.10$); Best2 $EC_{50} = 266$ nM ($logEC_{50} = 2.42 \pm 0.08$). *C,* relative anion permeability to I^-, NO_3^-, Br^-, and Glu^- compared with Cl^- ($n = 4–6$ cells for each condition). *D,* IC_{50} of CaCC in the three cell types for the anion channel blockers NFA, A9C, and DIDS ($n = 4–5$ for each condition; note log scale). *, $p < 0.05$.

(*e.g.* outward rectification and time dependence) and the amplitude of the Ca^{2+}-dependent Cl^- current in *Best2*$^{-/-}$ mice (*open symbols*) were generally similar to the Ca^{2+}-dependent Cl^- current in wild type cells (*filled symbols*, Fig. 4*A*). Furthermore, no significant changes were detected in the Ca^{2+} sensitivity of the CaCC current (Fig. 4*B*), the anion permeability sequence (Fig. 4*C*), or the sensitivity to the anion channel blockers NFA, A9C, and DIDS (Fig. 4*D*).

Best2 Expression in the Duct Cells of Mouse Submandibular Salivary Glands—The results shown in Figs. 3 and 4 demonstrated that the Best2 Ca^{2+}-activated Cl^- channel is not a major contributor to the formation of the endogenous Ca^{2+}-activated Cl^- channel in acinar cells and thus does not play a critical role in regulating salivary gland fluid secretion. However, Best2 may be expressed in submandibular gland duct cells where it could be important for NaCl absorption. *Best2*$^{-/-}$ mice were generated by substitution of *lacZ* for exons 1, 2, and part of exon 3 in the *Best2* gene (33), while leaving the *Best2* promoter intact. Accordingly, X-gal staining can be used to characterize the endogenous expression pattern of the *Best2* gene in the exocrine salivary gland. X-gal staining (blue) revealed that *Best2* was expressed in the duct cells of mouse submandibular glands, including granular, striated, and excretory duct cells (Fig. 5*A*, *left panel*). Note that X-gal staining rarely overlapped with immunoreactivity for Aqp5 (brown staining), a water channel whose expression is primarily restricted to the apical membrane of salivary gland acinar cells (6). No X-gal staining was detected in the submandibular glands of wild type mice (Fig. 5*A*, *right panel*).

Even though Best2 transcripts are present in salivary gland acinar cells (9), *Best2* promoter activity appeared to be considerably greater in submandibular gland duct cells (Fig. 5*A*). This raised the possibility that Best2 might be involved in regulating duct cell rather than acinar cell function in salivary glands. Acinar cells are well known to secrete a NaCl-rich saliva that is modified by passage through the ducts, *i.e.* duct cells reabsorb much of the NaCl secreted by the acini while secreting K^+ and HCO_3^- (for reviews, see Refs. 47, 49). Thus, we tested whether NaCl reabsorption was impaired in *Best2*$^{-/-}$ mice. However, there was no significant change in the Na^+, K^+, or Cl^- composition of the saliva generated by the submandibular gland in *Best2* null mice (Fig. 5*B*). The Best2 channel is also highly permeable to HCO_3^- (50). Because the HCO_3^- concentration for the most part determines the saliva pH, we measured pH as an index of HCO_3^- secretion. No significant difference was noted in saliva pH, suggesting that Best2 does not play a major role in HCO_3^- secretion in the mouse SMG (*Best2*$^{+/+}$, pH = 8.1 ± 0.1; *Best2*$^{-/-}$, pH = 8.3 ± 0.1, $n = 6$ in each group, $p > 0.1$).

Voltage clamp experiments were next performed using the standard whole-cell patch clamp technique to test for CaCC-like current in single submandibular granular duct cells, which are easily distinguishable from acinar cells by means of their distinctive morphology (37). Identical experimental conditions as in Fig. 1 were used to activate the CaCC current in duct cells. Despite the robust promoter activity of the *Best2* gene in submandibular duct cells (Fig. 5*A*), the characteristic Cl^- current generated by Ca^{2+}-activated Cl^- channels was not detected in granular duct cells (Fig. 5*C*, *inset*). In contrast to the strong outward rectification of the CaCC current typically observed at 250 nM internal free Ca^{2+} in acinar cells (see Fig. 1*A*), the Cl^- current in duct cells displayed inward rectification that was relatively insensitive to the CaCC blocker NFA (Fig. 5*C*, *main panel*).

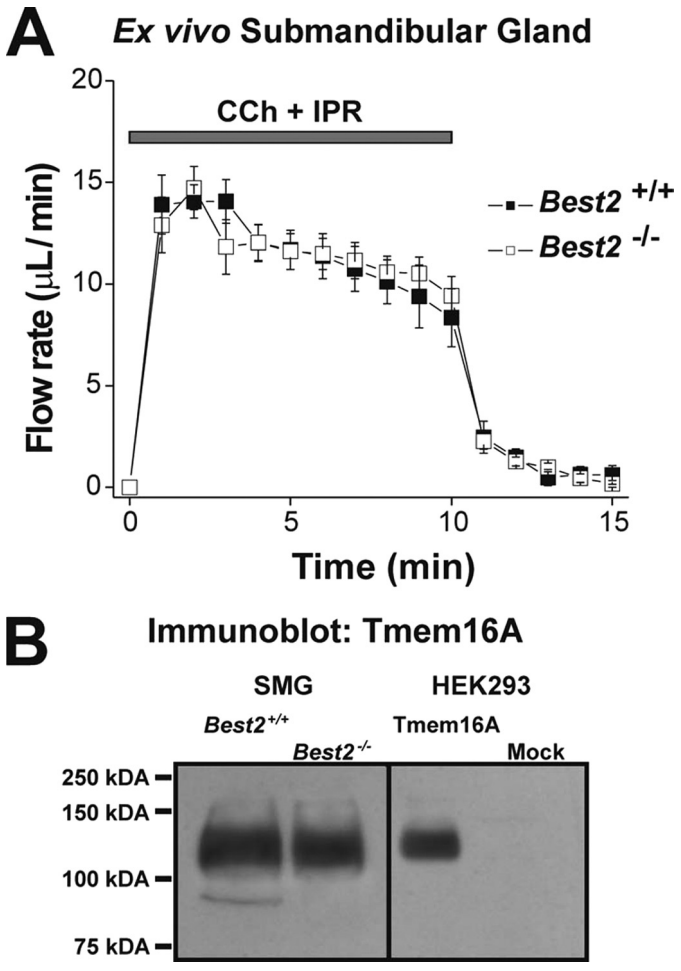

FIGURE 3. ***Ex vivo* fluid secretion and Tmem16A protein expression in the submandibular gland of *Best2*$^{-/-}$ mice.** *A,* fluid secretion rate was determined in the *ex vivo*, perfused submandibular glands from adult wild type (*Best2*$^{+/+}$) and *Best2* knock-out (*Best2*$^{-/-}$) mice. Secretion was stimulated by vascular perfusion with carbachol (0.3 μM *CCh*) + isoproterenol (5 μM *IPR*) applied for 10 min as indicated by the bar (*Best2*$^{+/+}$ $n = 9$ and *Best2*$^{-/-}$ $n = 9$ glands; no significant difference). *B,* Western blot analysis using an anti-Tmem16A antibody was performed as described under "Experimental Procedures" on plasma membrane protein isolated from wild type (*Best2*$^{+/+}$), *Best2* knock-out (*Best2*$^{-/-}$) mice, and HEK293 cells transiently transfected with either Tmem16A or empty vector. Estimated size of Tmem16A from its amino acid sequence = 110.9 kDa.

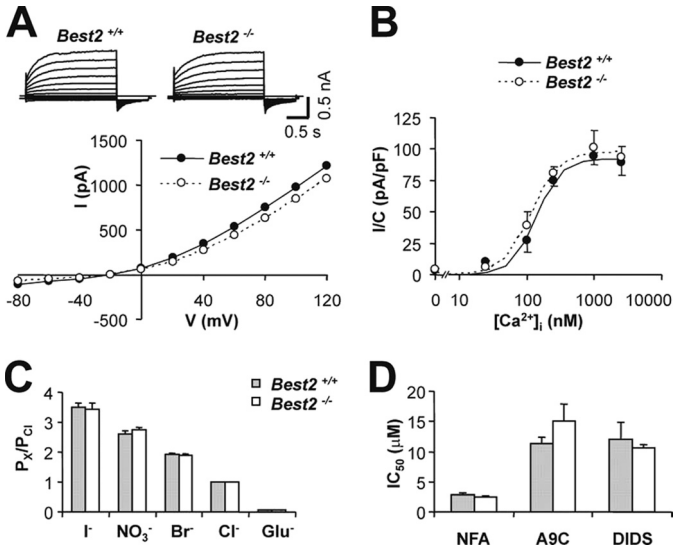

FIGURE 4. **CaCC current in submandibular acinar cells was unchanged in *Best2*$^{-/-}$ mice.** Submandibular gland acinar cells were isolated from adult *Best2*$^{+/+}$ and *Best2*$^{-/-}$ mice and the CaCC recorded as described in Fig. 1. *A,* representative raw current traces recorded with pipette solution buffered to 250 nM free [Ca^{2+}]. The time course of the currents is shown in the *upper panels,* and the current-voltage relations are shown in the *lower panel*. *B,* dependence of the CaCC current on internal [Ca^{2+}] was evaluated using concentrations ranging from near 0 to 2500 nM ($n = 4$–15 for each condition). *Best2*$^{+/+}$ EC_{50} = 134 nM ($logEC_{50}$ = 2.13 ± 0.21); *Best2*$^{-/-}$ EC_{50} = 116 nM ($logEC_{50}$ = 2.07 ± 0.30). *C,* anion permeability to I^-, NO_3^-, Br^-, and glutamate relative to Cl^- ($n = 4$–6 for each condition). *D,* IC_{50} of native CaCC for the anion channel blockers NFA, A9C, and DIDS ($n = 4$–5 for each condition).

Apical Expression of the Tmem16A Channel in Submandibular Acinar Cells—The above results demonstrated that Best2 is not involved in fluid secretion or NaCl reabsorption, suggesting instead that Tmem16A may be critical in one or both of these processes. The Tmem16A Cl^- channel was recently shown to be targeted to the apical pole of mouse submandibular gland acinar cells (6). However, another study found that Tmem16A is primarily expressed in the cytosol of mouse submandibular gland duct cells with no apparent apical staining of acinar cells (51). To address this apparent contradiction, we next performed immunolocalization studies to verify the localization of Tmem16A channels in the mouse submandibular gland. Tmem16A-dependent immunostaining was associated with proacinar and acinar cells in the glands of young and adult wild type mice (Fig. 6, *A, left panel,* and *B*, respectively). Note also that a prominent luminal staining was detected in intercalated ducts of the adult gland (Fig. 6*A*, *arrows*). At the subcellular level, most of the immunostaining was confined to the apical pole of acinar cells, consistent with the fluid secretion model (47). No specific staining was found in submandibular gland tissue from *Tmem16A*$^{-/-}$ mice (Fig. 6*A*, *right panel*). Thus, our results are consistent with an apical distribution of Tmem16A in the mouse submandibular gland as described previously (6).

Tmem16A-deficient Mice Lack Ca^{2+}-activated Cl^- Current and Stimulated Cl^- Efflux in Submandibular Acinar Cells—The apical targeting of Tmem16A suggested that this channel may generate the CaCC current critical for fluid secretion in submandibular gland acinar cells. To test this hypothesis, we next used mice lacking Tmem16A to determine whether this channel is critical for generating the CaCC current in submandibular gland acinar cells. PCR primers failed to amplify the 5′-deleted region of *Tmem16A* in *Tmem16A*$^{-/-}$ mice, confirming that intact Tmem16A transcript is not generated (34). *Tmem16A*$^{-/-}$ mice die shortly after birth, generally in less than 4 days (34). Thus, we isolated submandibular gland acinar cells from 2- to 3-day-old mice for patch clamp experiments.

The whole-cell CaCC current activated by 250 nM internal Ca^{2+} was recorded during voltage clamp steps from −80 to +120 in 20-mV steps from a holding potential of −50 mV in submandibular gland acinar cells from 2- to 3-day-old control mice. The time dependence for the activation of the currents (*upper panel*, Fig. 7*A*) and the current-voltage relation (*lower panel*, *filled symbols,* Fig. 7*A*) were virtually identical to those detected under identical conditions in adult submandibular gland acinar cells (compare with Fig. 1*A*). The CaCC current in young SMG acinar cells was inhibited >90% by the Ca^{2+}-activated Cl^- channel blocker NFA (100 μM, *middle* and *lower*

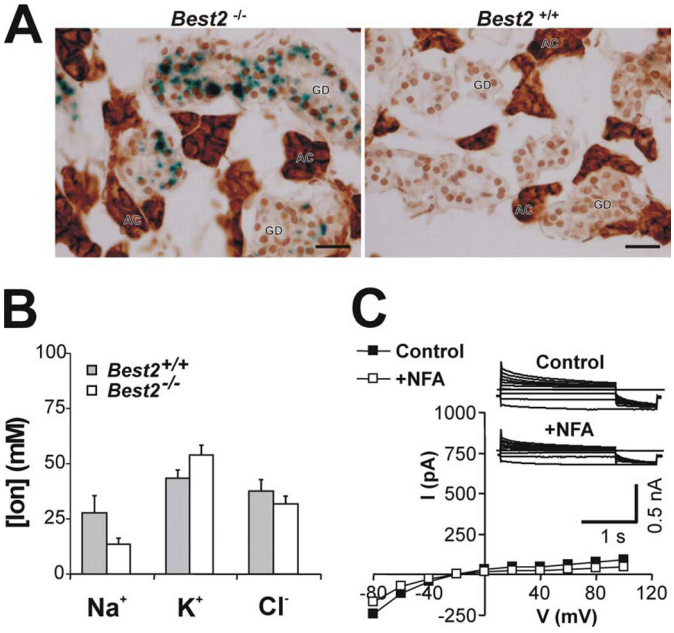

FIGURE 5. **Characterization of Best2 in submandibular gland duct cells.** *Best2* promoter activity, saliva ion composition, and the Cl^- current in granular duct cells from *Best2*$^{-/-}$ mice were examined. *A,* X-gal staining (*blue*) of *Best2* promoter-driven expression of LacZ and acinar Aqp5 immunolabeling (*brown*) in mouse submandibular glands from *Best2* null (*Best2*$^{-/-}$) and wild type (*Best2*$^{+/+}$) mice. *Bars,* 50 μm. *AC,* acinar cells; *GD,* granular duct cells. *B,* Na^+, K^+, and Cl^- composition of saliva collected from *ex vivo*, perfused submandibular glands was determined for wild type (*Best2*$^{+/+}$) and *Best2* knock-out (*Best2*$^{-/-}$) mice (see Fig. 3*A*; *Best2*$^{+/+}$ $n = 9$ and *Best2*$^{-/-}$ $n = 9$ glands; no significant differences). *C, inset,* internal Ca^{2+} concentration of 250 nM was used to activate CaCC current in mouse submandibular granular duct cells (as used for SMG acinar cells). Currents were recorded during 2-s voltage steps from −80 to +100 in 20-mV steps (from a holding potential of −50 mV) followed by 0.5-s step to −80 mV. *C,* Cl^- current plotted is from the end of the pulse *versus* voltage. Note that the Cl^- currents in submandibular granular duct cells were relatively insensitive to the Ca^{2+}-activated Cl^- channel blocker NFA (100 μM) and lacked the characteristic time and outward rectifying voltage dependence typical for CaCC ($n = 6$).

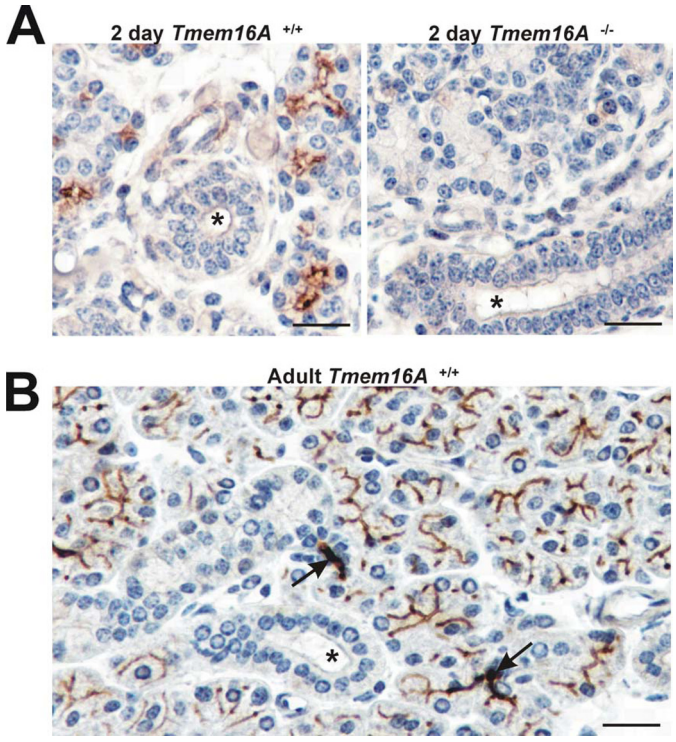

FIGURE 6. **Immunohistochemical localization of Tmem16A channel protein in young and adult mouse submandibular glands.** Immunoperoxidase labeling for Tmem16A in submandibular glands from young 2-day-old (*A, left panel*) and adult (*B*) *Tmem16A*$^{+/+}$ mice. Sections show staining of acinar cells with no apparent immunolabeling in duct cells, with the exception of strong staining of the intercalated cells in the adult gland (*arrows*). *A, right panel*, immunostaining is not present in submandibular glands from young 2-day-old *Tmem16A*$^{-/-}$ mice. *Asterisks* show luminal spaces. *Bars,* 50 μm.

panels, *open symbols*, Fig. 7*A*), as noted in adult submandibular acinar cells (see Fig. 1*A*). In contrast, acinar cells from *Tmem16A*$^{-/-}$ mice failed to express CaCC current, even when internal Ca^{2+} was raised well beyond 250 nM by addition of the Ca^{2+}-permeable ionophore ionomycin (Fig. 7*B*). In fact, the observed current density in acinar cells from *Tmem16A*$^{-/-}$ mice was equivalent to the expected background current. Together, these results suggested that the same CaCC is likely responsible for generating the Ca^{2+}-activated Cl^- current in the acinar cells of both young and adult mice. Composite results are summarized in Fig. 7*C* for experiments like those shown for individual cells in Fig. 7, *A* and *B*.

Our results demonstrate that *Tmem16A* encodes a critical component of the CaCC in salivary acinar cells, and accordingly, it likely plays a major role in the fluid secretion process. However, because *Tmem16A*$^{-/-}$ mice generally die in less than 4 days, we were unable to directly test this hypothesis in knockout mice. Instead, we monitored in submandibular acinar cells from 2- to 3-day-old mice the carbachol-stimulated efflux of Cl^-, an index of Cl^--driven fluid secretion (45, 47, 49). Fig. 8*A* shows that stimulation with this Ca^{2+}-mobilizing agonist caused a loss of intracellular Cl^- content in submandibular acinar cells isolated from *Tmem16A*$^{+/+}$ and *Tmem16A*$^{+/-}$ mice (*filled symbols*). In contrast, carbachol failed to elicit Cl^- efflux in submandibular acinar cells isolated from *Tmem16A*$^{-/-}$ mice (Fig. 8*A*, *open symbols*). Fig. 8*B* shows a summary of the data in Fig. 8*A* (*Tmem16A*$^{+/+}$ and *Tmem16A*$^{+/-}$; 0.10 ± 0.02 $\Delta F_0/F$, $N = 6$ animals, $n = 8$ experiments *versus* *Tmem16A*$^{-/-}$; 0.01 ± 0.01 $\Delta F_0/F$, $N = 4$ animals, $n = 8$ experiments, $p < 0.01$). One possible mechanism for the absence of Cl^- efflux in response to stimulation in *Tmem16A*$^{-/-}$ mice is that calcium mobilization might be impaired. However, carbachol induced a comparable increase in the intracellular [Ca^{2+}] in submandibular acinar cells isolated from *Tmem16A*$^{+/+}$ and *Tmem16A*$^{+/-}$ mice (Fig. 8*C*, *filled symbols*) and *Tmem16A*$^{-/-}$ mice (Fig. 8*C*, *open symbols*). Thus, the Ca^{2+} signaling machinery was intact in *Tmem16A*$^{-/-}$ mice, but no Cl^- efflux occurred, consistent with the Tmem16A channel being critical for fluid secretion in the mouse submandibular gland. Fig. 8*D* summarizes the results from Fig. 8*C* (*Tmem16A*$^{+/+}$ and *Tmem16A*$^{+/-}$; 0.16 ± 0.03 Δ ratio units, $N = 10$ animals, $n = 10$ experiments *versus* *Tmem16A*$^{-/-}$; 0.14 ± 0.03 Δ ratio units, $N = 4$ animals, $n = 4$ experiments, $p > 0.7$).

The Ca^{2+}-activated Cl^- channel blocker NFA (100 μM) inhibited the Tmem16A CaCC current expressed in HEK293 cells (Fig. 1*B*) as well as the CaCC currents in acinar cells isolated from both adult and young mice (Figs. 1*A* and 7*A*, respectively). To further test the prediction that Tmem16A activity is essential for fluid secretion in adult glands, we evaluated whether NFA would inhibit salivation in the *ex vivo* mouse sub-

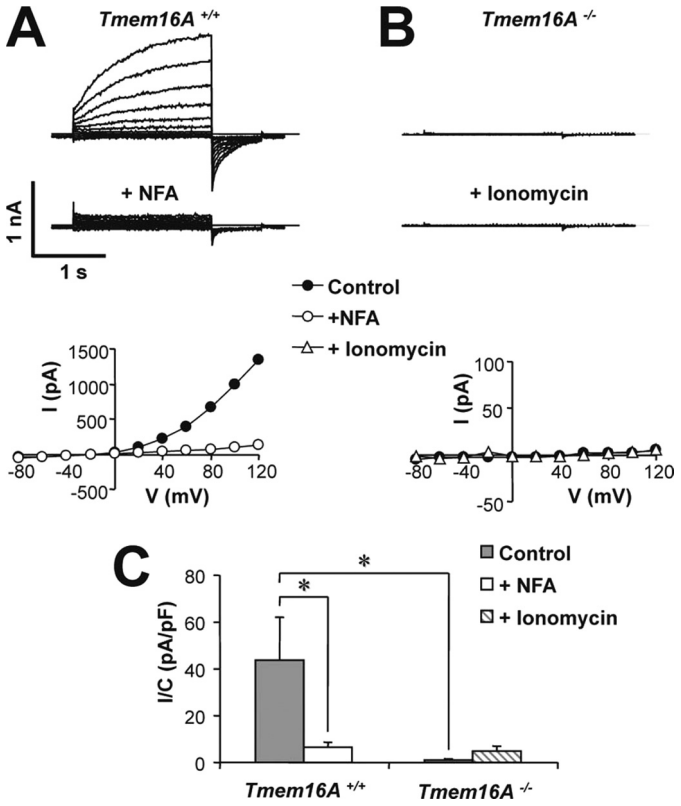

FIGURE 7. **Lack of CaCC current in submandibular acinar cells from *Tmem16A*$^{-/-}$ mice.** Submandibular gland acinar cells were isolated from 2- to 3-day-old *Tmem16A*$^{+/+}$ and *Tmem16A*$^{-/-}$ littermate mice, and the CaCC was recorded as described for Fig. 1 with pipette solution buffered to 250 nM free [Ca^{2+}]. *A,* representative raw current traces recorded from *Tmem16A*$^{+/+}$ mice. The time course of the currents and their sensitivity to 100 μM NFA are shown in the *upper panel* and the current-voltage relations are shown in the *lower panel*. *B,* representative raw current traces recorded from *Tmem16A*$^{-/-}$ mice. No current was observed in cells from knock-out animals even after superfusion with a Ca^{2+} ionophore (1 μM ionomycin, extracellular [Ca^{2+}] was 2 mM). *C,* summary of results showing the average amplitude of the CaCC currents recorded in acinar cells from *Tmem16A*$^{+/+}$ and *Tmem16A*$^{-/-}$ mice and their sensitivity to NFA or ionomycin (records were obtained from $n = 10$ and 27 cells obtained from $N = 3$ and 6 wild type and knock-out animals, respectively; from which 5 and 15 cells were tested with NFA or ionomycin, respectively). *, $p < 0.05$. Ionomycin-treated *Tmem16A*$^{-/-}$ cells were not significantly different from *Tmem16A*$^{-/-}$ cells.

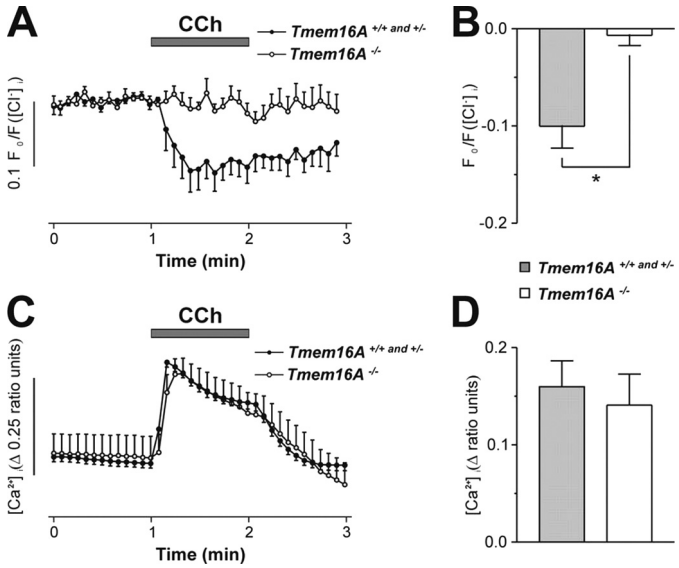

FIGURE 8. **Loss of carbachol-induced Cl^- efflux in submandibular acinar cells from *Tmem16A*$^{-/-}$ mice.** Intracellular [Cl^-] and [Ca^{2+}] were monitored as described under "Experimental Procedures." Data were collected at 1-s intervals but averaged over 5 s for clarity and presented as the mean ± S.E. *A,* submandibular acinar cells were isolated from *Tmem16A*$^{+/+,\ +/-}$ or *Tmem16A*$^{-/-}$ mice (2–3 days old), loaded with the chloride-sensitive dye SPQ, and stimulated with the calcium-mobilizing agonist carbachol (0.3 μM *CCh*) for 1 min where indicated by the *bar*. Data from *Tmem16A*$^{+/+}$ and *Tmem16A*$^{+/-}$ mice were combined for analysis because no differences in the responses to CCh were noted. *Traces* shown are the average of all experiments. *B,* summary of the results shown in *A* demonstrating the average change in F_0/F during stimulation. F_0/F values were generated by subtracting the average F_0/F value of the prestimulation period (between 0.5 and 1.0 min) from the average F_0/F value after achieving maximal Cl^- loss during the stimulation period (between 1.5 and 2.0 min). The average $\Delta F_0/F$ for *Tmem16A*$^{+/+}$ and *Tmem16A*$^{+/-}$ was significantly larger than the $\Delta F_0/F$ for *Tmem16A*$^{-/-}$ mice ($N = 6$ animals (1 *Tmem16A*$^{+/+}$ and 5 *Tmem16A*$^{+/-}$), $n = 8$ experiments *versus* $N = 4$ *Tmem16A*$^{-/-}$ animals, $n = 8$ experiments, $p < 0.01$). *C,* submandibular acinar cells were isolated from *Tmem16A*$^{+/+}$, *Tmem16A*$^{+/-}$, or *Tmem16A*$^{-/-}$ mice (2–3 days old) and loaded with the calcium-sensitive dye Fura-2 and stimulated with 0.3 μM CCh for 1 min where indicated by the *bar*. *Traces* shown are the average of all experiments performed. *D,* summary of the results shown in *C* demonstrating the average change in ratio units over base line (average value between the stimulation period of 1–2 min minus the average value of the prestimulation period between 0 and 1 min). The average change for *Tmem16A*$^{+/+}$ and *Tmem16A*$^{+/-}$ mice was not significantly different from the values obtained from *Tmem16A*$^{-/-}$ mice ($N = 10$ animals (4 *Tmem16A*$^{+/+}$ and 6 *Tmem16A*$^{+/-}$), $n = 10$ experiments, 76 cells *versus* $N = 4$ *Tmem16A*$^{-/-}$ animals, $n = 4$ experiments, 38 cells, $p > 0.7$).

mandibular gland. Stimulated fluid secretion was inhibited by NFA by about 90% in wild type and *Best2*$^{-/-}$ mice (Fig. 9, *A* and *B*, respectively) after 7 min of exposure. The saliva flow rate after 10 min of stimulation was reduced from 8.3 ± 1.4 μl/min (control, no NFA added, $n = 8$) to 0.6 ± 0.2 μl/min (NFA-treated, $n = 6$) in *Best2*$^{+/+}$ mice and from 9.4 ± 0.9 μl/min (control, $n = 8$) to 1.0 ± 0.4 μl/min (NFA, $n = 6$) in *Best2*$^{-/-}$ mice. As noted above (Fig. 3*B*), the expression of Tmem16A did not increase to compensate for loss of Best2. Notably, NFA did not inhibit the carbachol-induced increase in the intracellular [Ca^{2+}] (Fig. 9*C*), consistent with NFA acting on the Tmem16A Ca^{2+}-activated Cl^- channel to inhibit fluid secretion. Together, these results are consistent with Tmem16A, and not Best2, being an essential component of the Ca^{2+}-activated Cl^- channel complex required for salivary fluid secretion.

DISCUSSION

Ca^{2+}-dependent Cl^- channels are fundamental to the function of numerous organ systems such as membrane potential regulation in excitable cells (52, 53) and fluid secretion by exocrine gland acinar cells (15–18). Nevertheless, unequivocal molecular identification of the CaCC in these various cell types is generally lacking. Two candidate CaCCs expressed in salivary glands are Best2 (9, 46) and Tmem16A (5, 6, 32), members of the bestrophin (also known as Best or Vmd2) and Tmem16 (also known as Ano) families of Ca^{2+}-activated Cl^- channels, respectively. Using identical experimental conditions, we found that heterologous expression of either mouse Best2 or Tmem16A in HEK293 cells produced Ca^{2+}-activated Cl^- current with properties very similar to the Ca^{2+}-activated Cl^- current found in native salivary acinar cells. Although these results demonstrated that heterologous expression of Best2 and Tmem16A produces Ca^{2+}-dependent Cl^- currents, a direct link between this activity and the CaCC currents in native cells had not been unequivocally established. Therefore, *Best2*$^{-/-}$ and *Tmem16A*$^{-/-}$ mice were used to test the possibility that

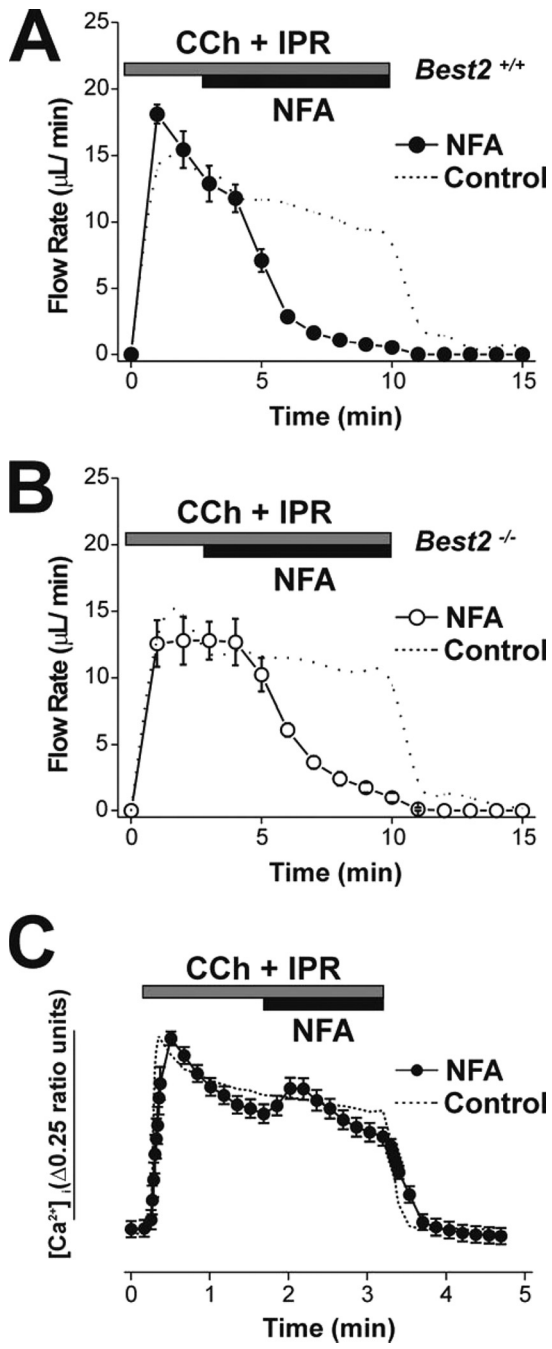

FIGURE 9. **NFA inhibited fluid secretion in the *ex vivo* submandibular gland of *Best2*$^{-/-}$ mice.** The fluid secretion rate was determined in the *ex vivo*, perfused submandibular glands from adult wild type (*A, Best2*$^{+/+}$, *filled symbols*) and *Best2* knock-out (*B, Best2*$^{-/-}$, *open symbols*) mice. Secretion was stimulated by vascular perfusion with carbachol (0.3 μM *CCh*) + isoproterenol (5 μM *IPR*) for 10 min where indicated by the *bar*. After 3 min of stimulation, fluid secretion was inhibited by addition of the Ca^{2+}-activated Cl^- channel blocker NFA (100 μM; *Best2*$^{+/+}$ $n = 9$ and *Best2*$^{-/-}$ $n = 9$ glands; no significant difference). Data in the absence of NFA (*dotted lines*) are the same as those in Fig. 3*A*. *C*, Fura-2 loaded SMG acinar cells were stimulated with 0.3 μM CCh + 5 μM isoproterenol for 3 min in the presence (*filled symbols*) or absence (*dotted line*) of NFA (100 μM) added 1.5 min after stimulation was initiated. Data were acquired every 1 s; however, for clarity the data are presented every 5 s ± S.E. with the exception of when the agonists were initially applied and just after removal. NFA did not significantly affect intracellular [Ca^{2+}] mobilization as there was no difference after 3 min of stimulation between control and NFA experiments (control = 0.16 ± 0.01 ratio units, *versus* NFA = 0.13 ± 0.01 ratio units, $n = 6$ and $n = 9$, respectively, $p > 0.6$). Data are presented as the average of 6 or more experiments per condition from $N = 3$ *Best2*$^{+/+}$ animals (control, $n = 6$ experiments, 16 cells; NFA, $n = 9$ experiments, 33 cells).

Best2 and/or Tmem16A generate the CaCC current in salivary gland acinar cells.

Although heterologous expression of Best2 produced a Ca^{2+}-activated Cl^- current with similar properties to those expressed in native salivary acinar cells, Best2 does not appear to be a critical molecular component of the Ca^{2+}-activated Cl^- channel complex in salivary gland acinar cells. *Best2* disruption did not alter the amplitude or properties of the Ca^{2+}-activated Cl^- current in native salivary gland acinar cells. Moreover, enhanced Tmem16A protein expression was not observed in *Best2* null mice, suggesting that Tmem16A did not compensate for loss of Best2 expression. Consistent with these observations, stimulated fluid secretion was normal in the *Best2*$^{-/-}$ submandibular gland, clearly demonstrating that Best2 does not play an important role in fluid secretion. Taken together, these results suggest that Best2 is a Ca^{2+}-dependent Cl^- channel, but it does not appear to represent the classical CaCC expressed in the exocrine salivary gland.

So what is the function of Best2 in salivary glands? X-gal staining revealed that the *Best2* promoter is highly active in the various types of duct cells of the mouse submandibular gland, implying that Best2 expression may be important for NaCl reabsorption in this organ. The cAMP-activated Cl^- channel cystic fibrosis transmembrane conductance regulator is likely the major apical Cl^- pathway in this process (54–56), but the molecular identity of the basolateral Cl^- pathway has not been determined. We therefore tested the possibility that Best2 is vital for NaCl reabsorption in *Best2* null mice. However, the ion composition of the saliva was not altered in mice lacking Best2. Indeed, patch clamp recordings failed to detect CaCC-like current in submandibular granular duct cells. Instead, the Cl^- current in these cells displayed two components. The first was a current with biophysical and pharmacological properties like VRAC, a cell volume-activated anion current (40, 41) that is very different from the outward rectifying, slowly developing CaCC current found in salivary gland acinar cells (15, 18). The second Cl^- current was activated at negative potentials in a time-dependent and NFA-insensitive manner, reminiscent of the inward rectifying Cl^- current in mouse submandibular duct cells that is inhibited by cadmium and is absent in *ClC-2* null mice (37). It is unclear why CaCC currents were not detected in duct cells because X-gal staining indicated that these cells express Best2. Considering that the sensitivity of the patch clamp technique is considerably more sensitive than X-gal staining, one possibility is that Best2 does not target to the plasma membrane of submandibular gland duct cells. Alternatively, *Best2* promoter activity might not correlate with protein expression, consistent with the lack of positive Best2 immunoreactivity in this tissue (data not shown).

Tmem16A was recently identified (4–6) as a new candidate for the Ca^{2+}-activated Cl^- channel in numerous tissues, including human (32) and mouse (5, 6, 23, 51) salivary glands. We found that functional expression of the Tmem16A variant cloned from the mouse submandibular gland produced CaCC currents in HEK293 cells with properties much like those in native mouse salivary acinar cells. This raised the possibility that Tmem16A is a functional Cl^- channel in salivary gland acinar cells and is necessary for saliva secretion. Indeed, Ous-

ingsawat *et al.* (51) showed that stimulation of submandibular acinar cells isolated from wild type and from *Tmem16A* knock-out mice results in a shift of the reversal potential of the ionic current in opposite directions. One interpretation of these results is that *Tmem16A* ablation diminished the contribution of Cl^- current to the total cell conductance. Also in submandibular acinar cells, knock-out of *Tmem16A* results in a smaller swelling-activated conductance, presumably through a Ca^{2+}-dependent process (23). However, *in vivo* disruption of Tmem16A expression resulted in a surprisingly small ~25% decrease in salivary gland secretion (6). This rather modest effect on salivary gland function was likely due to the remaining expression of Tmem16A after *in vivo* small interfering RNA knockdown. Alternatively, it is possible that the native Ca^{2+}-activated Cl^- channel complex includes additional, as yet unidentified, protein components, possibly other members of the *Tmem16* gene family. Significantly, we demonstrate that the native Ca^{2+}-activated Cl^- current and Ca^{2+}-activated Cl^- efflux were absent in salivary acinar cells isolated from *Tmem16A* null mice. In agreement with these observations, the Tmem16A channel inhibitor NFA nearly abolished saliva secretion in mouse submandibular glands. Collectively, our findings demonstrate in salivary gland acinar cells that Tmem16A is a major component of the Ca^{2+}-activated Cl^- channel complex required for stimulated Cl^- efflux and fluid secretion.

Acknowledgments—We thank Laurie Koek, Yasna Jaramillo, Chun Pfahnl, and Margarit Sievert for excellent technical assistance and Alaka Srivastava for cloning the mouse submandibular gland Best2 transcript. We thank Ted Begenisich and Catherine Ovitt for helpful discussions during the course of this work and for critical reading of the manuscript.

REFERENCES

1. Barro Soria, R., Spitzner, M., Schreiber, R., and Kunzelmann, K. (2009) *J. Biol. Chem.* **284,** 29405–29412
2. Duta, V., Duta, F., Puttagunta, L., Befus, A. D., and Duszyk, M. (2006) *J. Membr. Biol.* **213,** 165–174
3. Kunzelmann, K., Milenkovic, V. M., Spitzner, M., Soria, R. B., and Schreiber, R. (2007) *Pflugers Arch.* **454,** 879–889
4. Caputo, A., Caci, E., Ferrera, L., Pedemonte, N., Barsanti, C., Sondo, E., Pfeffer, U., Ravazzolo, R., Zegarra-Moran, O., and Galietta, L. J. (2008) *Science* **322,** 590–594
5. Schroeder, B. C., Cheng, T., Jan, Y. N., and Jan, L. Y. (2008) *Cell* **134,** 1019–1029
6. Yang, Y. D., Cho, H., Koo, J. Y., Tak, M. H., Cho, Y., Shim, W. S., Park, S. P., Lee, J., Lee, B., Kim, B. M., Raouf, R., Shin, Y. K., and Oh, U. (2008) *Nature* **455,** 1210–1215
7. Stöhr, H., Heisig, J. B., Benz, P. M., Schöberl, S., Milenkovic, V. M., Strauss, O., Aartsen, W. M., Wijnholds, J., Weber, B. H., and Schulz, H. L. (2009) *J. Neurosci.* **29,** 6809–6818
8. Qu, Z., Fischmeister, R., and Hartzell, C. (2004) *J. Gen. Physiol.* **123,** 327–340
9. Srivastava, A., Romanenko, V. G., Gonzalez-Begne, M., Catalán, M. A., and Melvin, J. E. (2008) *J. Membr. Biol.* **222,** 43–54
10. Tsunenari, T., Sun, H., Williams, J., Cahill, H., Smallwood, P., Yau, K. W., and Nathans, J. (2003) *J. Biol. Chem.* **278,** 41114–41125
11. Hartzell, H. C., Qu, Z., Yu, K., Xiao, Q., and Chien, L. T. (2008) *Physiol. Rev.* **88,** 639–672
12. Qu, Z., and Hartzell, C. (2004) *J. Gen. Physiol.* **124,** 371–382
13. Suzuki, M., Morita, T., and Iwamoto, T. (2006) *Cell. Mol. Life Sci.* **63,** 12–24
14. Pifferi, S., Dibattista, M., and Menini, A. (2009) *Pflugers Arch.* **458,** 1023–1038
15. Arreola, J., Melvin, J. E., and Begenisich, T. (1996) *J. Gen. Physiol.* **108,** 35–47
16. Evans, M. G., and Marty, A. (1986) *J. Physiol.* **378,** 437–460
17. Ishikawa, T. (1996) *J. Membr. Biol.* **153,** 147–159
18. Zeng, W., Lee, M. G., and Muallem, S. (1997) *J. Biol. Chem.* **272,** 32956–32965
19. Gruber, A. D., Schreur, K. D., Ji, H. L., Fuller, C. M., and Pauli, B. U. (1999) *Am. J. Physiol.* **276,** C1261–1270
20. Huang, P., Liu, J., Di, A., Robinson, N. C., Musch, M. W., Kaetzel, M. A., and Nelson, D. J. (2001) *J. Biol. Chem.* **276,** 20093–20100
21. Suzuki, M., and Mizuno, A. (2004) *J. Biol. Chem.* **279,** 22461–22468
22. Hartzell, H. C., Yu, K., Xiao, Q., Chien, L. T., and Qu, Z. (2009) *J. Physiol.* **587,** 2127–2139
23. Almaça, J., Tian, Y., Aldehni, F., Ousingsawat, J., Kongsuphol, P., Rock, J. R., Harfe, B. D., Schreiber, R., and Kunzelmann, K. (2009) *J. Biol. Chem.* **284,** 28571–28578
24. Duta, V., Szkotak, A. J., Nahirney, D., and Duszyk, M. (2004) *FEBS Lett.* **577,** 551–554
25. Marmorstein, L. Y., Wu, J., McLaughlin, P., Yocom, J., Karl, M. O., Neussert, R., Wimmers, S., Stanton, J. B., Gregg, R. G., Strauss, O., Peachey, N. S., and Marmorstein, A. D. (2006) *J. Gen. Physiol.* **127,** 577–589
26. Stöhr, H., Marquardt, A., Nanda, I., Schmid, M., and Weber, B. H. (2002) *Eur. J. Hum. Genet.* **10,** 281–284
27. Sun, H., Tsunenari, T., Yau, K. W., and Nathans, J. (2002) *Proc. Natl. Acad. Sci. U.S.A.* **99,** 4008–4013
28. Rock, J. R., and Harfe, B. D. (2008) *Dev. Dyn.* **237,** 2566–2574
29. Krämer, F., Stöhr, H., and Weber, B. H. (2004) *Cytogenet. Genome Res.* **105,** 107–114
30. Qu, Z., Cui, Y., and Hartzell, C. (2006) *FEBS Lett.* **580,** 2141–2146
31. Qu, Z. Q., Yu, K., Cui, Y. Y., Ying, C., and Hartzell, C. (2007) *J. Biol. Chem.* **282,** 17460–17467
32. Gonzalez-Begne, M., Lu, B., Han, X., Hagen, F. K., Hand, A. R., Melvin, J. E., and Yates, J. R. (2009) *J. Proteome Res.* **8,** 1304–1314
33. Bakall, B., McLaughlin, P., Stanton, J. B., Zhang, Y., Hartzell, H. C., Marmorstein, L. Y., and Marmorstein, A. D. (2008) *Invest. Ophthalmol. Vis. Sci.* **49,** 1563–1570
34. Rock, J. R., Futtner, C. R., and Harfe, B. D. (2008) *Dev. Biol.* **321,** 141–149
35. Brown, D. A., and Yule, D. I. (2007) *Biochim. Biophys. Acta* **1773,** 166–175
36. Bullard, T., Koek, L., Roztocil, E., Kingsley, P. D., Mirels, L., and Ovitt, C. E. (2008) *Dev. Biol.* **320,** 72–78
37. Romanenko, V. G., Nakamoto, T., Catalán, M. A., Gonzalez-Begne, M., Schwartz, G. J., Jaramillo, Y., Sepúlveda, F. V., Figueroa, C. D., and Melvin, J. E. (2008) *Am. J. Physiol. Gastrointest. Liver Physiol.* **295,** G1058–G1067
38. Nakamoto, T., Romanenko, V. G., Takahashi, A., Begenisich, T., and Melvin, J. E. (2008) *Am. J. Physiol. Cell Physiol.* **294,** C810–C819
39. Romanenko, V. G., Nakamoto, T., Srivastava, A., Begenisich, T., and Melvin, J. E. (2007) *J. Physiol.* **581,** 801–817
40. Droogmans, G., Maertens, C., Prenen, J., and Nilius, B. (1999) *Br. J. Pharmacol.* **128,** 35–40
41. Eggermont, J., Trouet, D., Carton, I., and Nilius, B. (2001) *Cell Biochem. Biophys.* **35,** 263–274
42. Hille, B. (1992) *Ionic Channels of Excitable Membranes*, 2nd Ed., pp. 344–387, Sinauer Associates Inc., Sunderland, MA
43. Hancock, A. A., Bush, E. N., Stanisic, D., Kyncl, J. J., and Lin, C. T. (1988) *Trends Pharmacol. Sci.* **9,** 29–32
44. Nakamoto, T., Brown, D. A., Catalán, M. A., Gonzalez-Begne, M., Romanenko, V. G., and Melvin, J. E. (2009) *J. Biol. Chem.* **284,** 4815–4822
45. Foskett, J. K. (1990) *Am. J. Physiol.* **259,** C998–C1004
46. Nakamoto, T., Srivastava, A., Romanenko, V. G., Ovitt, C. E., Perez-Cornejo, P., Arreola, J., Begenisich, T., and Melvin, J. E. (2007) *Am. J. Physiol. Regul. Integr. Comp. Physiol.* **292,** R2380–R2390
47. Melvin, J. E., Yule, D., Shuttleworth, T., and Begenisich, T. (2005) *Annu. Rev. Physiol.* **67,** 445–469

48. Qu, Z., Chien, L. T., Cui, Y., and Hartzell, H. C. (2006) *J. Neurosci.* **26,** 5411–5419
49. Cook, D. I., Van Lennep, E. W., Roberts, M. L., and Young, J. A. (eds) (1994) *Secretion by the Major Salivary Glands*, 3rd Ed., pp. 1061–1117, Raven Press, Ltd., New York
50. Qu, Z., and Hartzell, H. C. (2008) *Am. J. Physiol. Cell Physiol.* **294,** C1371–C1377
51. Ousingsawat, J., Martins, J. R., Schreiber, R., Rock, J. R., Harfe, B. D., and Kunzelmann, K. (2009) *J. Biol. Chem.* **284,** 28698–28703
52. Frings, S., Reuter, D., and Kleene, S. J. (2000) *Prog. Neurobiol.* **60,** 247–289
53. Large, W. A., and Wang, Q. (1996) *Am. J. Physiol.* **271,** C435–C454
54. Lee, M. G., Choi, J. Y., Luo, X., Strickland, E., Thomas, P. J., and Muallem, S. (1999) *J. Biol. Chem.* **274,** 14670–14677
55. Zeng, W., Lee, M. G., Yan, M., Diaz, J., Benjamin, I., Marino, C. R., Kopito, R., Freedman, S., Cotton, C., Muallem, S., and Thomas, P. (1997) *Am. J. Physiol.* **273,** C442–C455
56. Catalán, M. A., Nakamoto, T., Gonzalez-Begne, M., Camden, J. M., Wall, S. M., Clarke, L. L., and Melvin, J. E. (2010) *J. Physiol.* **588,** 713–724